Analysis of composite material interface crack face contact and friction effects using a new node-pairs contact algorithm*

Zhong Zhi-Peng(钟志鹏)[a], He Yu-Bo(何郁波)[b], and Wan Shui(万 水)[a]†

[a] School of Transportation, Southeast University, Nanjing 210096, China
[b] Department of Mathematics, Huaihua University, Huaihua 418008, China

(Received 5 September 2013; revised manuscript received 29 October 2013; published online 20 April 2014)

A new node-pairs contact algorithm is proposed to deal with a composite material or bi-material interface crack face contact and friction problem (e.g., resistant coating and thermal barrier coatings) subjected to complicated load conditions. To decrease the calculation scale and calculation errors, the local Lagrange multipliers are solved only on a pair of contact nodes using the Jacobi iteration method, and the constraint modification of the tangential multipliers are required. After the calculation of the present node-pairs Lagrange multiplier, it is turned to next contact node-pairs until all node-pairs have finished. Compared with an ordinary contact algorithm, the new local node-pairs contact algorithm is allowed a more precise element on the contact face without the stiffness matrix singularity. The stress intensity factors (SIFs) and the contact region of an infinite plate central crack are calculated and show good agreement with those in the literature. The contact zone near the crack tip as well as its influence on singularity of stress fields are studied. Furthermore, the frictional contacts are also considered and found to have a significant influence on the SIFs. The normalized mode-II stress intensity factors $\hat{K}_{\rm II}$ for the friction coefficient decrease by 16% when f changes from 1 to 0.

Keywords: contact and friction, node-pairs contact algorithm, interface crack, mixed mode loading stress intensity factors

PACS: 46.50.+a, 46.55.+d, 72.80.Tm **DOI:** 10.1088/1674-1056/23/6/064601

1. Introduction

As the key materials of turbines for propulsion and power generation, thermal barrier coatings (TBCs) have been used to protect turbine engine blades from high temperatures, which enables modern gas-turbine engines to work at high temperatures (∼ 1600 °C), and improve the thermal efficiency of gas-turbine engines to 60%.[1–4] However, the structure of a thermal barrier-coated component contains four layers (see Fig. 1) in general:[4] (i) the substrate, (ii) the bond coat, (iii) the thermally grown oxide (TGO), and (iv) the ceramic top coat. Different physical properties (e.g., elasticity modulus, coefficient of thermal expansion) of each layer cause the stress focusing on the interface of dissimilar materials under thermo-mechanics loadings. Moreover, there exists interface damage lying at the interface of biomaterials (see Fig. 2) caused by thermal fatigue, which enhances the concentration of stress.[5] Several failures, such as delamination and cracking, will appear at the interface and/or in the adhesive layer, causing the degradation and fracture of the substrate.[5–8] Therefore, it is necessary to develop an accurate analytic method of solving the bimaterial interface crack problem, which could make a contribution to the interface failure studies of the TBC.[9–25]

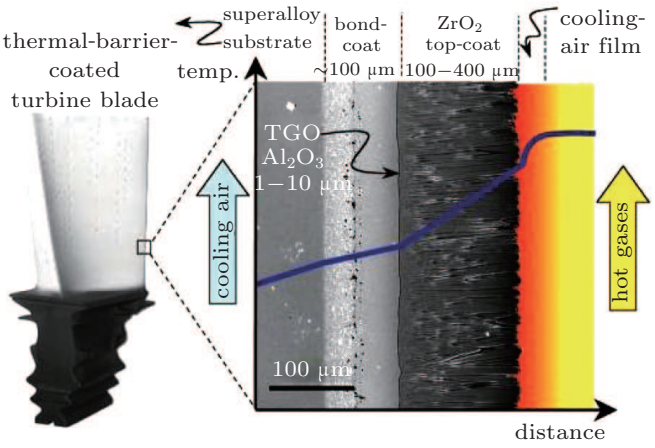


Fig. 1. (color online) Turbine blade with TBCs and cross section of TBCs.[4]

Williams[12] performed an asymptotic analysis of the elastic fields at the tip of an open interface crack, and found that the stresses are of an oscillatory manner and the upper and lower surfaces of the crack should wrinkle and overlap near the ends of the crack, when the crack surfaces are assumed to be traction-free. Erdogan[13] and England[14] proposed the same analytical solutions. Sih and Asaro[15] proposed plastic stress fields at the tip of the interface cracks to eliminate the oscillatory manner. This unsatisfactory feature is also eliminated by Comninou[16] via introducing contact zones at the tips of an interface crack. Comninou suggested that the in-

*Project supported by the National Basic Research Program of China (Grant No. 2012CB026200) and the National Natural Science Foundation of China (Grant No. 50878048).

†Corresponding author. E-mail: lanyu421@163.com

© 2014 Chinese Physical Society and IOP Publishing Ltd

terface crack is not fully opened, but that its two faces are in contact with each other near the crack tips. Gautesen and Dundurs[17] solved Comninou's equation exactly, but their solution is quite complicated. Later, Gautesen[18] reduced the problem into an eigenvalue problem and obtained relatively simple approximate expressions for the physical quantities of interest. Although significant progress has been made in asymptotic fields, few solutions are available for a partially open interface crack with a large scale of contact. Therefore, a series of numerical approaches have been applied to deal with contact and friction problems. Among these methods, the finite-element method has been applied to closed interfacial crack problems. van der Zande and Grootenboer[19] employed a hybrid finite-element method and Lagrange multipliers to handle the crack contact at interface crack tips. Lee and Gao[20] developed a hybrid finite-element technique combined with Lagrange multipliers to model cracks in anisotropic materials with closed interfacial crack tips. Giner *et al.*[21] used the extended finite-element method (X-FEM) based on the use of Lagrange multiplier elements to establish the contact and calculate K_{II}. Elguedj *et al.*[22] adopted a mixed augmented Lagrangian-extended finite-element method to model the elastic–plastic fatigue crack problem. When the crack surfaces are under combined compression and shear loads, the effect of contact stress on the crack surfaces cannot always be ignored. To eliminate the crack surface penetrations, the Lagrange multiplier method mentioned above is typically used. However, a large number of additional unknown variables need to be included due to the introduction of Lagrange multipliers as new variables in the traditional Lagrange multipliers method. It is still difficult to analyze the crack contact as the global stiffness matrix orders are too large for the finite-element method when the number of contact elements is huge. Furthermore, the generated global stiffness matrix is difficult to solve for singularity. A complex and tedious iterative algorithm was commonly used for analyzing the contact problem in previous studies, which is not suitable for engineering applications.[26]

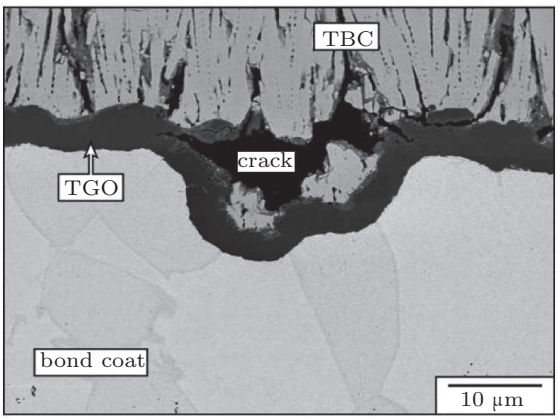


Fig. 2. Interface determination caused by thermal cycling.[5]

In this study, a new node-pairs contact algorithm is presented for the analysis of a bimaterial interface crack face contact and friction problem subjected to complicated load conditions (e.g., coating, thermal barrier coatings). To decrease the calculation scale and calculation errors, the local Lagrange multipliers are solved only on a pair of contact nodes using the Jacobi iteration method firstly, and the constraint modification of the tangential multipliers are required. After the calculation of the present node-pairs Lagrange multiplier, we turn to the contact node-pairs until all node-pairs are finished. Once the Lagrange multipliers of all node-pairs are completed, the displacement is calculated at last. Compared with ordinary contact algorithms, the new local node-pairs contact algorithm is condensed on every node pair to avoid the calculation of the global stiffness matrix. In addition, as the generated stiffness matrix of each node pair is no longer singular, the contact force can be solved iteratively without special treatment. According to the algorithm, the nonlinear finite-element program was compiled. Numerical results are given for an interface crack in an infinite bimaterial plate under remote combined loading. Comparison between the FEM solution and the analytical solution shows that the node-pairs contact algorithm is more effective than traditional algorithms in terms of computer storage, calculation accuracy, and rate of convergence. Finally, we compare the solutions with those obtained when the crack surface interpenetration is not prevented, in an effort to illustrate the significance of including crack surface friction and contact for interface crack problems.

2. FEM model accounting for contact at the crack interface

2.1. Minimum potential energy principle of the fracture problem with contact along the crack faces

We consider two bodies, a master (target) body $\Omega^{(\mathrm{t})}$ and a slave body $\Omega^{(\mathrm{s})}$, as shown in Fig. 3. The local coordinates are established on the crack surface. Let $\boldsymbol{u}^{(\mathrm{t})}$ and $\boldsymbol{u}^{(\mathrm{s})}$ be the displacement field solution on region $\Omega^{(\mathrm{t})}$ and $\Omega^{(\mathrm{s})}$, respectively. The normal and tangential relative displacements between the crack faces Γ_{c} are defined as[26–28]

$$g_n = \left(\boldsymbol{u}^{(\mathrm{t})}\Big|_{\Gamma_{\mathrm{c}}} - \boldsymbol{u}^{(\mathrm{s})}\Big|_{\Gamma_{\mathrm{c}}} \right) \cdot \boldsymbol{n}, \tag{1}$$

$$g_\tau = \left(\boldsymbol{u}^{(\mathrm{t})}\Big|_{\Gamma_{\mathrm{c}}} - \boldsymbol{u}^{(\mathrm{s})}\Big|_{\Gamma_{\mathrm{c}}} \right) \cdot \boldsymbol{s}, \tag{2}$$

where $\boldsymbol{n}$ and $\boldsymbol{s}$ are the outward normal and tangential vectors to the surface. Let p_n and $\boldsymbol{p}_\tau$ be the normal and tangential load acting on the contact point.

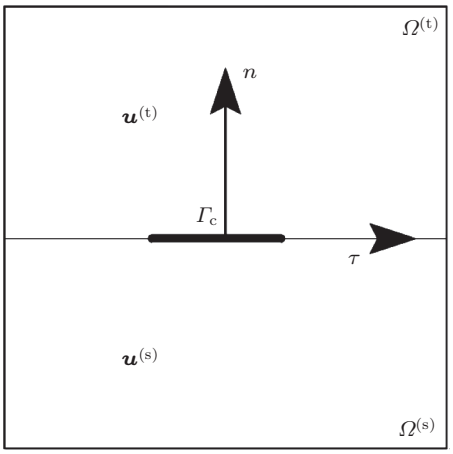


Fig. 3. Local coordinate on crack surface.

The normal contact conditions may be expressed in the standard Kuhn–Tucker form as[26,29]

$$p_n \geq 0, \quad g_n \geq 0, \quad p_n g_n = 0, \tag{3}$$

where $p_n \geq 0$ means that if there is contact, then the pressure is compressive. The expression $p_n g_n = 0$ requires that the pressure is nonzero only when the contact occurs, i.e., $g_n = 0$. Furthermore, when $g_n > 0$, this condition requires p_n to be zero, consistent with an out-of-contact condition.

The tangential contact constraints are also obtained from the Kuhn–Tucker conditions for Coulomb friction[21,26,29]

$$\begin{aligned} &\|\boldsymbol{p}_\tau\| - f p_n \leq 0, \quad g_\tau - \xi \frac{\boldsymbol{p}_\tau}{\|\boldsymbol{p}_\tau\|} = 0, \\ &\xi \geq 0, \quad (\|\boldsymbol{p}_\tau\| - f p_n)\xi = 0, \end{aligned} \tag{4}$$

where f is the coefficient of friction. The expression $\|\boldsymbol{p}_\tau\| - f p_n \leq 0$ requires that the magnitude of the tangential stress vector does not exceed the product of the coefficient of friction and the contact pressure. The expressions

$$g_\tau - \xi \frac{\boldsymbol{p}_\tau}{\|\boldsymbol{p}_\tau\|} = 0$$

and $\xi \geq 0$ define the colinearity of slip velocity and frictional stress in rate form, and $(\|\boldsymbol{p}_\tau\| - f p_n)\xi = 0$ permits slipping to occur only when the magnitude of the tangential traction is equal to $f p_{\mathrm{n}}$.

Considering a region Ω with an arbitrary crack, a given load $\boldsymbol{T}$ along the Γ_σ and prescribed displacement $\boldsymbol{u}_{\mathrm{d}}$ along the Γ_{d} are shown in Fig. 4. The potential energy Π_{p} expressed as the sum of the elastic strain energy, the cohesive energy, and the work of external forces[19,26]

$$\begin{aligned} \Pi_{\mathrm{p}} = &\int_\Omega 1/2\boldsymbol{\varepsilon}^{\mathrm{T}} \boldsymbol{D}\boldsymbol{\varepsilon}\,\mathrm{d}\Omega - \int_\Omega \boldsymbol{f}^{\mathrm{T}}\boldsymbol{u}\,\mathrm{d}\Omega \\ &- \int_{\Gamma_{\mathrm{c}}} \boldsymbol{p}^{\mathrm{T}}(\boldsymbol{u}^{(\mathrm{t})} - \boldsymbol{u}^{(\mathrm{s})})\,\mathrm{d}\Gamma - \int_{\Gamma_\sigma} \boldsymbol{T}^{\mathrm{T}}\boldsymbol{u}\,\mathrm{d}\Gamma, \end{aligned} \tag{5}$$

where $\boldsymbol{D}$ is the given elastic matrix, $\boldsymbol{\varepsilon} = \boldsymbol{L}\boldsymbol{u}$ is the strain vector, $\boldsymbol{L}$ is the differential operator, $\boldsymbol{u}$ is the whole displacement field, $\boldsymbol{f}$ is the body force, $\boldsymbol{p} = (p_n, p_{\tau_1}, p_{\tau_2})^{\mathrm{T}}$ is the contact force on Γ_{c}, $\boldsymbol{T}$ is the boundary traction, and T denotes the transposition. The contact force $\boldsymbol{p}$ on Γ_{c}, which are treated as independent variables in the present problem, can also be viewed mathematically as Lagrange multipliers $\boldsymbol{\lambda}$.

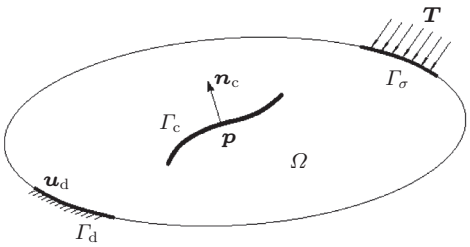


Fig. 4. Fracture problem with an arbitrary crack and boundary conditions.

The actual displacement is characterized by an optimality condition: it is a local minimum of the potential energy.[28,30] By minimization of the potential energy Eq. (5) and combination of Eq. (3) and Eq. (4), we find $\boldsymbol{u}$ and $\boldsymbol{\lambda}$ satisfy

$$\begin{cases} \min\limits_{\boldsymbol{u},\boldsymbol{\lambda}} (\int_\Omega 1/2\boldsymbol{\varepsilon}^{\mathrm{T}}\boldsymbol{D}\boldsymbol{\varepsilon}\,\mathrm{d}\Omega - \int_\Omega \boldsymbol{f}^{\mathrm{T}}\boldsymbol{u}\,\mathrm{d}\Omega \\ \quad - \int_{\Gamma_{\mathrm{c}}} \boldsymbol{\lambda}^{\mathrm{T}}(\boldsymbol{u}^{(\mathrm{t})} - \boldsymbol{u}^{(\mathrm{s})})\,\mathrm{d}\Gamma - \int_{\Gamma_\sigma} \boldsymbol{T}^{\mathrm{T}}\boldsymbol{u}\,\mathrm{d}\Gamma), \\ \lambda_n \geq 0, \ \|\boldsymbol{\lambda}_\tau\| \leq f\lambda_n, \end{cases} \tag{6}$$

where λ_n is the normal Lagrange multiplier, and $\boldsymbol{\lambda}_\tau = (\lambda_{\tau_1}, \lambda_{\tau_2})^{\mathrm{T}}$ is the tangential Lagrange multiplier vector for the three-dimensional space.

2.2. Finite-element discretization dedicated to contact along the crack faces[27,31–34]

The finite-element method (FEM) is based on the partition of unity concept.[32] For a mechanical or physical problem, after the mathematical model is determined, the computational domain is discretized by a series of elements with regular shape in FEM. Then the potential energy of the system is the sum of potential energy of all elements, and equation (6) is rewritten as

$$\begin{cases} \min\limits_{\boldsymbol{u},\boldsymbol{\lambda}} \Big(\sum\limits_e \big(\int_{\Omega_e} \frac{1}{2}\boldsymbol{\varepsilon}\mathbf{D}\boldsymbol{\varepsilon}\,\mathrm{d}\Omega\big) - \sum\limits_e \big(\int_{\Omega_e} \boldsymbol{f}^{\mathrm{T}}\boldsymbol{u}\,\mathrm{d}\Omega\big) \\ \quad - \sum\limits_e \Big(\int_{\Gamma_{\mathrm{c}}^e} \boldsymbol{\lambda}^{\mathrm{T}}(\boldsymbol{u}^{(\mathrm{t})} - \boldsymbol{u}^{(\mathrm{s})})\,\mathrm{d}\Gamma\Big) \\ \quad - \sum\limits_e \Big(\int_{\Gamma_\sigma^e} \boldsymbol{T}^{\mathrm{T}}\boldsymbol{u}\,\mathrm{d}\Gamma\Big)\Big), \\ \lambda_n \geq 0, \ \|\boldsymbol{\lambda}_\tau\| \leq f\lambda_n. \end{cases} \tag{7}$$

The FEM displacement field approximation solution $\boldsymbol{u}$ is given by

$$\boldsymbol{u} = \sum_{i=1}^{m} \boldsymbol{N}_i \boldsymbol{u}_i^e = \boldsymbol{N}u^e, \tag{8}$$

where

$$\boldsymbol{N}_i = \begin{bmatrix} N_i & & \\ & N_i & \\ & & N_i \end{bmatrix}$$

is the interpolation function matrix, and N_i $(i = 1,2,\ldots,m)$ is the element linear shape functions basis of the three-dimensional (3D) finite elements space.

$$\boldsymbol{u}_i^e = \begin{bmatrix} u_i^e & v_i^e & w_i^e \end{bmatrix}^{\mathrm{T}}$$

is the displacement vector of the element node i, $\boldsymbol{N} = [\boldsymbol{N}_1\ \boldsymbol{N}_2\ \cdots\ \boldsymbol{N}_m]$ and $\boldsymbol{u}^e = [\boldsymbol{u}_1^e\ \boldsymbol{u}_2^e\ \cdots\ \boldsymbol{u}_m^e]^{\mathrm{T}}$. m is the node number of space elements.

The crack interface is composed of two-dimensional elements, which are sub-elements resulting from three-dimensional elements cut by the crack and called here the interface elements. The interface is discretized by integration points. The field of Lagrange multipliers $\boldsymbol{\lambda}$ are defined on interface elements[27,34]

$$\boldsymbol{\lambda} = \sum_{i=1}^{k} \boldsymbol{\Phi}_i \boldsymbol{\lambda}_i^e = \boldsymbol{\Phi}\boldsymbol{\lambda}^e, \tag{9}$$

where $\boldsymbol{\Phi}_i = \begin{bmatrix} \Phi_i & & \\ & \Phi_i & \\ & & \Phi_i \end{bmatrix}$ is the interpolation function matrix, and Φ_i $(i = 1,2,\ldots,k)$ is the element dual linear shape functions basis of the two-dimensional (2D) interface elements space. $\boldsymbol{\lambda}_i^e = \begin{bmatrix} \lambda_{in} & \lambda_{i\tau_1} & \lambda_{i\tau_2} \end{bmatrix}^{\mathrm{T}}$ is the Lagrange multipliers vector of the element node i with 3 degrees of freedom per Gauss point, $\boldsymbol{\Phi} = [\boldsymbol{\Phi}_1\ \boldsymbol{\Phi}_2\ \cdots\ \boldsymbol{\Phi}_{\mathrm{k}}]$, $\boldsymbol{\lambda}^e = \left[\boldsymbol{\lambda}_1^e\ \boldsymbol{\lambda}_2^e\ \cdots\ \boldsymbol{\lambda}_{\mathrm{k}}^e\right]^{\mathrm{T}}$. The k is the the Gauss node number of interface element.

From Eq. (8), after the determination of displacement field $\boldsymbol{u}$, the strain field $\boldsymbol{\varepsilon}$ solved by geometric equation is given by

$$\boldsymbol{\varepsilon} = \boldsymbol{L}\boldsymbol{u} = \boldsymbol{L}\boldsymbol{N}\boldsymbol{u}^e = \boldsymbol{B}\boldsymbol{u}^e, \tag{10}$$

where $\boldsymbol{B}$ is the strain matrix.

By introducing transition matrix $\boldsymbol{G}$, the element node displacement array $\boldsymbol{u}^e$ is expressed by the structure node displacement array $\boldsymbol{U}$

$$\boldsymbol{u}^e = \boldsymbol{G}\boldsymbol{U}, \tag{11}$$

where $\boldsymbol{U} = [u_1\ v_1\ w_1\ \cdots u_i\ v_i\ w_i\ \cdots\ u_{\mathrm{n}}\ v_{\mathrm{n}}\ w_{\mathrm{n}}]^{\mathrm{T}}$, and n is the total node number of structure.

In the same way, the element node Lagrange multiplier array $\boldsymbol{\lambda}^e$ is replaced by structure node displacement array $\boldsymbol{\Lambda}$ by introducing transition matrix $\boldsymbol{S}$

$$\boldsymbol{\lambda}^e = \boldsymbol{S}\boldsymbol{\Lambda}, \tag{12}$$

where

$$\boldsymbol{\Lambda} = \begin{bmatrix} \lambda_{1n}\ \lambda_{1\tau_1}\ \lambda_{1\tau_2}\ \cdots\ \lambda_{in}\ \lambda_{i\tau_1}\ \lambda_{i\tau_2}\ \cdots\ \lambda_{sn}\ \lambda_{s\tau_1}\ \lambda_{s\tau_2} \end{bmatrix}^{\mathrm{T}},$$

s is the total Gauss node number of crack faces. Introducing Eq. (12), (11), the strain field Eq. (10) and the discretized quantities on the crack faces Eq. (9) in Eq. (7), we obtain the discretized equation as

$$\begin{cases} \min\limits_{\boldsymbol{U},\boldsymbol{\Lambda}} \big(1/2\boldsymbol{U}^{\mathrm{T}}\sum\limits_e(\boldsymbol{G}^{\mathrm{T}}\boldsymbol{K}^e\boldsymbol{G})\boldsymbol{U} - \boldsymbol{U}^{\mathrm{T}}\sum\limits_e(\boldsymbol{G}^{\mathrm{T}}\boldsymbol{F}^e) \\ \quad -\boldsymbol{\Lambda}^{\mathrm{T}}\sum\limits_e(\boldsymbol{S}^{\mathrm{T}}\boldsymbol{P}^e\boldsymbol{G})\boldsymbol{B}\boldsymbol{U}\big), \\ \lambda_{in} \geq 0, \|\boldsymbol{\lambda}_{i\tau}\| \leq f\lambda_{in}, \end{cases} \tag{13}$$

where $\boldsymbol{K}^e = \int_{\Omega^e} \boldsymbol{B}^{\mathrm{T}}\boldsymbol{D}\boldsymbol{B}\,\mathrm{d}\Omega$ is the element stiffness matrix, the load array of element equivalent node is $\boldsymbol{F}^e = \int_{\Omega^e} \boldsymbol{N}^{\mathrm{T}}\boldsymbol{f}\,\mathrm{d}\Omega + \int_{\Gamma_\sigma^e} \boldsymbol{N}^{\mathrm{T}}\boldsymbol{T}\,\mathrm{d}\Gamma$, the load array on the interface element is $\boldsymbol{P}^e = \int_{\Gamma_{\mathrm{c}}^e} \boldsymbol{\Phi}^{\mathrm{T}}\boldsymbol{N}\,\mathrm{d}\Gamma$, and $\boldsymbol{B}$ is the correlation matrix, which yields $\boldsymbol{B}\boldsymbol{U} = \boldsymbol{U}^{(\mathrm{t})} - \boldsymbol{U}^{(\mathrm{s})}$.

Then equation (13) can be rewritten as

$$\begin{cases} \min\limits_{\boldsymbol{U},\boldsymbol{\Lambda}} \left(\frac{1}{2}\boldsymbol{U}^{\mathrm{T}}\boldsymbol{K}\boldsymbol{U} - \boldsymbol{U}^{\mathrm{T}}\boldsymbol{A}\boldsymbol{\Lambda} - \boldsymbol{U}^{\mathrm{T}}\boldsymbol{F}\right), \\ \lambda_{in} \geq 0, \|\boldsymbol{\lambda}_{i\tau}\| \leq f\lambda_{in}, \end{cases} \tag{14}$$

where $\boldsymbol{K} = \sum\limits_e \boldsymbol{G}^{\mathrm{T}}\boldsymbol{K}^e\boldsymbol{G}$ is the global stiffness matrix, $\boldsymbol{A} = \sum\limits_e (\boldsymbol{S}^{\mathrm{T}}\boldsymbol{P}^e\boldsymbol{G})\boldsymbol{B}$ is the constraint matrix, and $\boldsymbol{F} = \sum\limits_e (\boldsymbol{G}^{\mathrm{T}}\boldsymbol{F}^e)$ is the nodal loads vector.

According to the variational principle,[33] equation (14) is equivalent to

$$\begin{cases} \boldsymbol{K}U - \boldsymbol{A}\boldsymbol{\Lambda} - \boldsymbol{F} = \boldsymbol{0}, \\ \boldsymbol{A}\boldsymbol{U} = \boldsymbol{0}, \\ \lambda_{in} \geq 0, \|\boldsymbol{\lambda}_{i\tau}\| \leq f\lambda_{in}. \end{cases} \tag{15}$$

2.3. Basic principle of the node-pairs Lagrange multiplier method for modeling crack contact and friction

Considering the i-th node pairs, the first formula in Eq. (15) is written as

$$\boldsymbol{K}_{ii}\boldsymbol{U}_i - \boldsymbol{A}_{ii}\boldsymbol{\lambda}_i = \boldsymbol{F}_i - \boldsymbol{K}_{ij}\boldsymbol{U}_{j,j\neq i} + \boldsymbol{A}_{ik}\boldsymbol{\lambda}_{i,i\neq k}, \tag{16}$$

where $\boldsymbol{K}_{ii} = \mathrm{diag}\,(k_{mm}\ k'_{mm}\ k''_{mm}\ k_{nn}\ k'_{nn}\ k''_{nn})$ is the stiffness matrix at the i-th node pairs, k_{mm}, k'_{mm}, k''_{mm}, k_{nn}, k'_{nn}, and k''_{nn} are the diagonal elements in the formed total stiff matrix.

$$\boldsymbol{A}_{ii} = \mathrm{diag}\left(a_{mm}\ a'_{mm}\ a''_{mm}\ a_{nn}\ a'_{nn}\ a''_{nn}\right) \tag{17}$$

is the diagonal matrix of stiffness matrix $\boldsymbol{A}$ at the i-th node pairs, $\boldsymbol{U}_i = [u_m\ v_m\ w_m\ u_n\ v_n\ w_n]^{\mathrm{T}}$ is the i-th node pairs displacement vector, $\boldsymbol{\lambda}_i = [\lambda_{mn}\ \lambda_{m\tau_1}\ \lambda_{m\tau_2}\ \lambda_{nn}\ \lambda_{n\tau_1}\ \lambda_{n\tau_2}]^{\mathrm{T}}$ is the Lagrange multipliers vector at the i-th node pairs, and m and n are the node number with regard to the i-th node pairs.

Combining the contact and friction constraint condition of node pairs, similar to Eq. (16), we solve the local Lagrange multiplier $\boldsymbol{\lambda}_i^l$ as follows:

$$\begin{cases} \boldsymbol{A}_{ii}^{\mathrm{T}}\boldsymbol{K}_{ii}^{-1}\boldsymbol{A}_{ii}\boldsymbol{S}_i^{\mathrm{T}}\boldsymbol{\lambda}_i^l = \boldsymbol{A}_{ii}^{\boldsymbol{T}}\boldsymbol{K}_{ii}^{-1}\boldsymbol{F}_i, \\ \lambda_{in}^l \geq 0, \|\boldsymbol{\lambda}_{i\tau}^l\| \leq f_i\lambda_{in}^l, \end{cases} \tag{18}$$

where $\boldsymbol{\lambda}_i^l = \boldsymbol{S}_i\boldsymbol{\lambda}_i$, and $\boldsymbol{S}_i$ is the transition matrix from global coordinate to local coordinate.

In the problem of Eq. (18), the Jacobi iteration method is adopted to solve $\boldsymbol{\lambda}_i^l$. During the solving process, a modification of normal and tangential multipliers under the inequality constraints in the second formula of Eq. (18) is described as

$$\begin{cases} \text{if } \lambda_{in}^l \leq 0, & \boldsymbol{\lambda}_i^l = \boldsymbol{0}; \\ & \text{when } \left\|\boldsymbol{\lambda}_{i\tau}^l\right\| \geq f\lambda_{in}^l, \\ \text{if } \lambda_{in}^l > 0, & \text{then } \boldsymbol{\lambda}_{i\tau}^l = f_i\lambda_{in}^l \frac{\lambda_{i\tau}^l}{\left\|\lambda_{i\tau}{}^l\right\|}; \\ & \text{when } \left|\boldsymbol{\lambda}_{i\tau}^l\right| \leq f_i\boldsymbol{\lambda}_{i\tau}^l, \\ & \text{then } \boldsymbol{\lambda}_{i\tau}^l = \boldsymbol{\lambda}_{i\tau}^l, \end{cases} \tag{19}$$

where $\boldsymbol{\lambda}_i^l = \boldsymbol{T}_{ii}\boldsymbol{\lambda}_i$ when importing the transition matrix $\boldsymbol{T}_{ii}$, and $\boldsymbol{T}_{ii}$ is the transition matrix from global coordinate to local coordinate.

After the calculation of all point multipliers, the Lagrange multipliers are substituted into the equation $\boldsymbol{KU} - \boldsymbol{A\Lambda} - \boldsymbol{F} = \boldsymbol{0}$. An incomplete factorization technique is used to solve displacement $\boldsymbol{U}$. The computation of Lagrange multipliers and displacement is iterative, until the error precision required can be attained.

The iterative algorithm of frictional contact is described as follows:

i) Extraction of $\boldsymbol{K}_{ii}$, $\boldsymbol{A}_{ii}$, and $\boldsymbol{S}_i$. The subscript i denotes the i-th node pairs.

ii) Initialization of iterative step $p = 0$, multipliers $\boldsymbol{\lambda}^1 = \boldsymbol{0}$ and $\boldsymbol{\lambda} = \boldsymbol{0}$, displacement $\boldsymbol{U} = \boldsymbol{0}$, and stopping criterion ε_1 and ε_2 for iteration.

iii) Calculation of $\left(\bar{\boldsymbol{\lambda}}_i^l\right)^p$ $(i = 1, 2, \ldots, s)$ one by one using the Jacobi iteration method and correction of $(\bar{\boldsymbol{\lambda}}_i^l)^p = (\bar{\boldsymbol{\lambda}}_i^l)^p + \gamma((\bar{\boldsymbol{\lambda}}_i^l)^p - (\bar{\boldsymbol{\lambda}}_i^l)^{p-1})$ through the Uzawa algorithm, where γ $(0 < \gamma < 1)$ is the automatical modification through a nonlinear iteration algorithm. The iterative errors $\mathrm{err} = \left\|\left\{\bar{\boldsymbol{\lambda}}_i^l\right\}^p - (\bar{\boldsymbol{\lambda}}_i^l)^{p-1}\right\|_{L^2}$ are calculated and the local multipliers $(\bar{\boldsymbol{\lambda}}_i^l)^p$ are transformed into global multipliers $(\bar{\boldsymbol{\lambda}}_i)^p$.

iv) By substituting $(\bar{\boldsymbol{\lambda}}_i)^p$ $(i = 1, 2, \ldots, s)$ into $\boldsymbol{KU} - \boldsymbol{A\Lambda} - \boldsymbol{F} = \boldsymbol{0}$, the displacements $\boldsymbol{U}^p$ are solved iteratively based on an incomplete factorization technique and the iteration error $\mathrm{ERR} = \left\|\boldsymbol{U}^p - \boldsymbol{U}^{p-1}\right\|_{L^2}$ is calculated.

v) Convergence judgments. If the convergence result ($\mathrm{err} \le \varepsilon_1$ or $\mathrm{ERR} \le \varepsilon_2$) is achieved, we stop the calculation; otherwise, we set $p = p + 1$ and go to step iii).

In the above procedure, the stiff matrices $\boldsymbol{K}_{ii}$, $\boldsymbol{A}_{ii}$, and $\boldsymbol{S}_i$ need to be formed only once at the first step of iteration. The right-hand vectors are updated at each following iterative step. As the Lagrange multiplier and displacement are solved respectively, this could decrease the calculation scale and prevent the diagonal matrix from being zero. More importantly, as the Lagrange multipliers solved node-pairs, the requirement of computer storage is not high and the size of elements on the contact surface could be very small.

3. Stress intensity factors of an interface crack with frictional contact

The asymptotic problem of interface cracks with sliding friction was first studied by Comninou for interface cracks.[9,16] The main feature of their results is that the singular stress field near a closed crack tip is quite different from the oscillatory singular field of an open crack. The interfacial tractions in the front of the interface and behind the tip of a crack lying on the interface between two dissimilar, linear-elastic, anisotropic materials (see Fig. 5) are given by[10,35]

$$\sigma_{r\theta}(r,0) = \sigma_{xy}(r,0) = K_{\mathrm{II}}(2\pi r)^{\omega-1}, \tag{20}$$

$$\sigma_{\theta\theta}(r,\pi) = \sigma_{yy}(r,\pi) = K_{\mathrm{II}}(2\pi r)^{\omega-1}\beta\sin(\omega\pi), \tag{21}$$

$$\begin{aligned}\sigma_{r\theta}(r,\pi) &= \sigma_{xy}(r,\pi) = -K_{\mathrm{II}}(2\pi r)^{\omega-1}\cos\omega\pi \\ &= -K_{\mathrm{II}}(2\pi r)^{\omega-1} sf\beta\sin\omega\pi,\end{aligned} \tag{22}$$

where K_{II} is the mode II stress intensity factor,

$$\beta = \frac{\mu_1(\kappa_2 - 1) - \mu_2(\kappa_1 - 1)}{\mu_1(\kappa_2 + 1) + \mu_2(\kappa_1 + 1)}$$

is a Dundurs parameter, μ_i $(i = 1, 2)$ are the shear moduli for the media, and

$$\kappa_i = \begin{cases} 3 - 4\nu_i, & \text{for plane strain,} \\ \dfrac{3 - \nu_i}{1 + \nu_i}, & \text{for plane stress,} \end{cases} \tag{23}$$

where ν_i are the Poisson ratios, and subscripts (i = 1, 2) stand for upper and lower materials, respectively. The ω is the minimal eigenvalue of $\cot\omega\pi = sf\beta$. The proper choice of $s = \pm 1$ induces correspondence between the shear stress and tangential shift directions at the point of application, so that $\mathrm{sgn}(\sigma_{xy}) = \mathrm{sgn}(\Delta u_x)$.

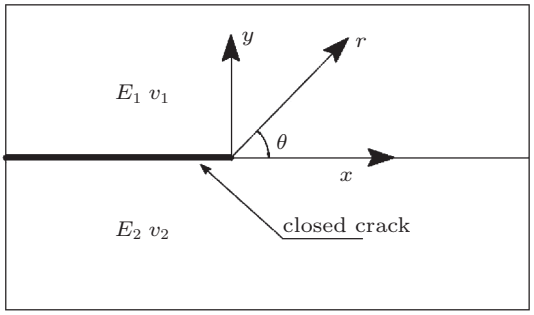


Fig. 5. Interface crack and coordinate system.

The displacement field along the crack face ($\theta = \pi$) can be deduced as

$$\begin{aligned}\Delta u_r &= -\Delta u_x \equiv u_{1r}(\theta = \pi) - u_{2r}(\theta = -\pi) \\ &= -AK_{\mathrm{II}}(2\pi)^{2\omega-1}\left(\frac{r}{2\pi}\right)^{\omega}\sin\omega\pi,\end{aligned} \tag{24}$$

where

$$A = \frac{1}{4\omega}\left[\frac{(\kappa_1 - 1)(1 + \beta) + 2}{\mu_1} + \frac{(\kappa_2 - 1)(1 - \beta) + 2}{\mu_2}\right].$$

The individual SIF at the crack tip can be obtained based on the stress distribution around the crack tip as

$$K_{\mathrm{II}} = (2\pi r)^{1-\omega}\sigma_{xy}(r,0). \tag{25}$$

The individual SIF at the crack tip can be determined from the displacement field as

$$K_{\mathrm{II}} = \lim\frac{(2\pi)^{1-\omega}}{A\sin\omega\pi}\frac{\Delta u_x(r)}{r^{\omega}}. \tag{26}$$

When the stress and displacement fields near the crack tip are predicted from the FE simulation, the SIF at the crack tip

can be determined by the extrapolation method. The effective SIF $K_{\rm eff}$ and the phase angle ψ acting as fracture mechanics quantities for modeling the fracture process can be obtained, respectively, by[7,35]

$$K_{\rm eff} = \sqrt{K_{\rm I}^2 + K_{\rm II}^2}, \quad \psi = \operatorname{atan}\left(\frac{K_{\rm II}}{K_{\rm I}}\right). \tag{27}$$

4. Numerical example and discussion

4.1. Interface crack with frictionless contact

A center crack lying between two dissimilar isotropic media under combined shear and compressive loading (see Fig. 6) is used to examine the accuracy of the aforementioned technique. The plane is $2W = 20$ m with a $L = 2$ m crack. The a is the left crack opening length, and b is the right crack opening length, in which the x–y coordinate is located at the center of the crack. The mechanical properties of the upper materials are chosen as $E_1 = 35$ MPa, and $v_1 = 0$. The elastic modulus of the lower materials E_2 is determined according to $\beta = 0$, 0.1, 0.2, 0.3, 0.4, 0.5, and $v_2 = 0$. The applied shear stress S was assumed to be 0.1 MPa. The tension load is defined based on the tension/shear ratios (T/S) ranging from -0.4 to 0.4. A negative ratio that means compressive load is applied instead of tension. The friction coefficient is taken to be $f = 0$ (no friction). The finite-element mesh for the panels is depicted in Fig. 7. The width and the height near the contact boundary of the plate were taken to be 1000 times the crack length L. The plane strain was assumed for all FEM analyses in this study.

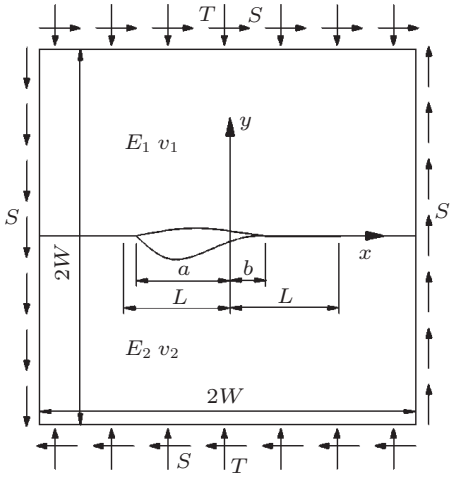


Fig. 6. Interface crack in a biomaterial infinite medium under combined loading.

Following Ref. [17], the normal gap is non-dimensionalized as

$$\Delta\bar{V} = \frac{C\Delta V}{PL},$$

where

$$C = \frac{2\mu_2(1+\alpha)}{(1-\beta^2)(\kappa_2+1)},$$

and $P = (T^2 + S^2)^{1/2}$.

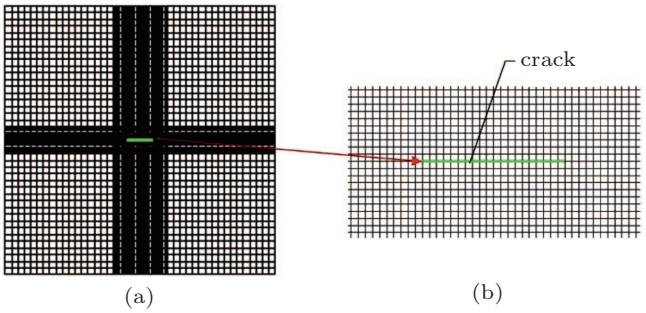


Fig. 7. (color online) Interface crack in infinite medium model: (a) whole plate and (b) crack surfaces.

Figures 8 and 9 show a comparison of some of the finite-element results with that in Ref. [17]. Excellent agreement is observed in Figs. 8 and 9. It may also be noted that as the ratio (T/S) ranges from -0.2 to 0.2, the tangential shift changes slightly, but the normal gap decreases and the contact region increases.

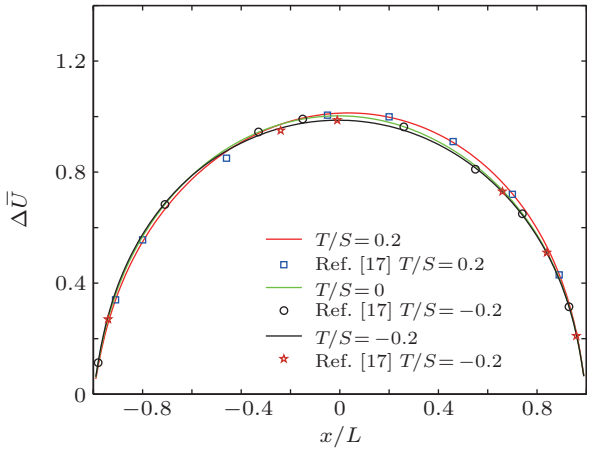


Fig. 8. (color online) Tangential shift along the crack for $\alpha = 1.0$ and $\beta = 0.25$.

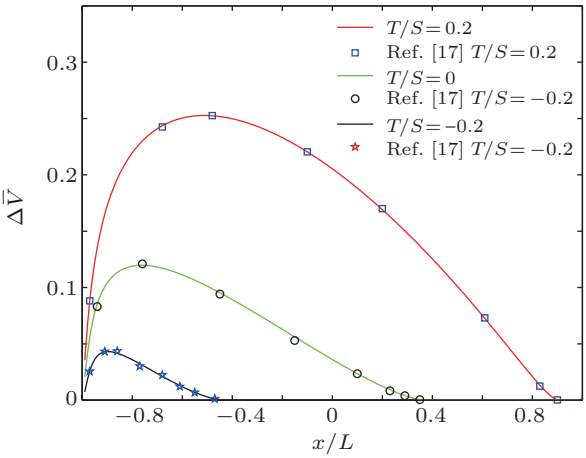


Fig. 9. (color online) Normal gap along the crack for $\alpha = 1.0$ and $\beta = 0.25$.

The results are given for five ratios of 0.4, 0.2, 0, -0.2, and -0.4. The variation of b/L, which determines the extension of the large contact zone, is shown in Table 1. The normalized mode II stress intensity factors $\hat{K}_{\rm II} = K_{\rm II}/\pi LP$ at

the crack tip with a large contact zone are also shown in Table 1. These results are compared with the previously reported results by Gautesen and Dundures,[18] and the maximum difference is less than 4%.

Table 1. Comparison of the large-scale contact b/L and $\hat{K}_{\rm II}$ at the right crack tip for $\alpha = 1.0$, $\beta = 0.25$, and those in Ref. [18].

T/S	This paper		Ref. [18]		Difference/%	
	b/L	$\hat{K}_{\rm II}$	b/L	$\hat{K}_{\rm II}$	b/L	$\hat{K}_{\rm II}$
–0.4	–0.740	0.915	–0.760	0.929	1.136	1.507
–0.2	–0.400	0.970	–0.426	0.982	1.823	1.222
0.0	0.390	1.030	0.379	1.007	2.903	2.284
0.2	0.870	1.045	0.909	1.013	3.491	3.159
0.4	0.950	1.028	0.990	1.013	4.040	1.481

Figure 10 shows the variation of the large contact zone sizes b/L with β. It is interesting to note that with the increase in β, the extent of the large contact zone may increase for $T/S < 0$ and decrease for $T/S > 0$. However, the value of b/L changes little for $T/S = 0$.

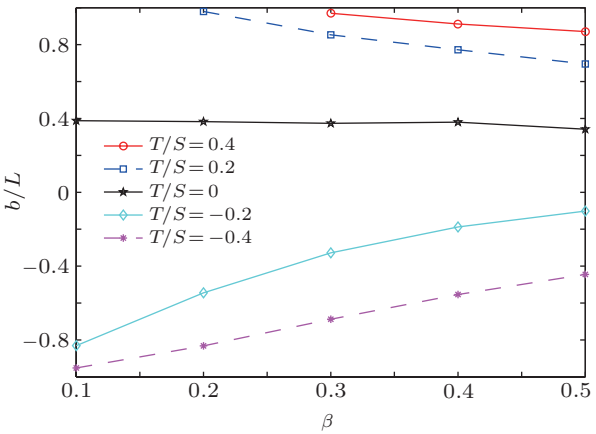


Fig. 10. (color online) Extent of the large contact zone b/L as a function of β.

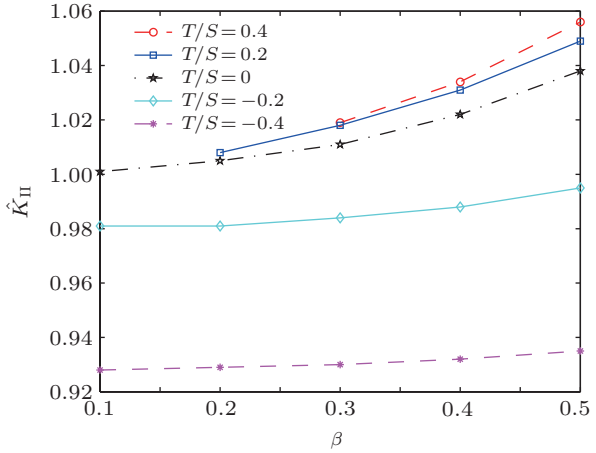


Fig. 11. (color online) Variation of $\hat{K}_{\rm II}$ with β at the crack tip with a large-scale contact.

The variation of the normalized mode II stress intensity factor at the tip with the large contact zone is shown in Fig. 11. The normalized mixed-mode stress-intensity factor $K_{\rm eff}/P\sqrt{\pi L}$ is plotted in Fig. 12. The theoretical solution is larger than numerical one, especially for $T/S = -0.4$, which demonstrates that the error arises when the large-scale crack surface contact is neglected.

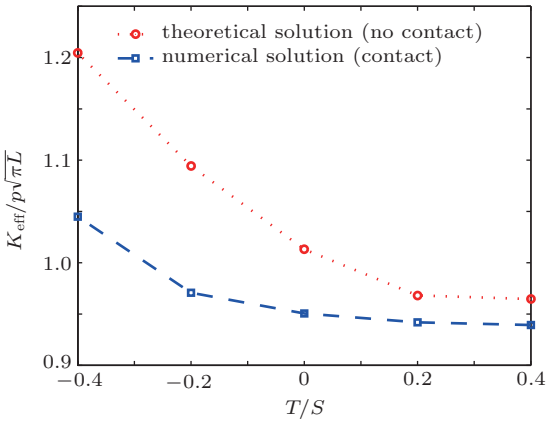


Fig. 12. (color online) Normalized mixed-mode stress-intensity factors at the left crack tip for $\beta = 0.25$.

4.2. Effect of friction coefficients

An open crack may be forced to close even if only the shear load is applied. The effect of friction force between the cracks of the upper and lower surfaces is investigated. The material properties are employed to attain $\alpha = 1$ and $\beta = 0.5$. The finite element mesh is shown in Fig. 5 and the friction coefficients are $f = 0.25$, 0.5, 0.75, and 1.0. The non-dimensional normal gaps $\bar{V}$ are plotted as curves in Fig. 13. Compared with Ref. [24], an excellent agreement is observed in Fig. 13. We can see the normal gaps $\Delta\bar{U}$ decrease and the contact zone increases with the friction coefficients. The normalized tangential shifts are plotted in Fig. 14. It may be noted that with increasing friction, the tangential shift decreases and the stress intensity factors decrease (see Fig. 15). The size of contact zone increases from 0.66 to 0.83 when the friction coefficient changes from $f = 0$ to $f = 1.0$. The normalized stress intensity factor $\hat{K}_{\rm II}$ decreases from 1.03 to 0.86 when the friction coefficient changes from $f = 0$ to $f = 1.0$.

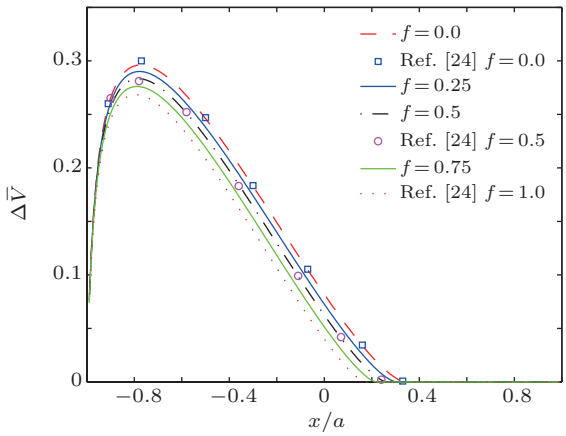


Fig. 13. (color online) Normal gaps for $\alpha = 1$ and $\beta = 0.5$.

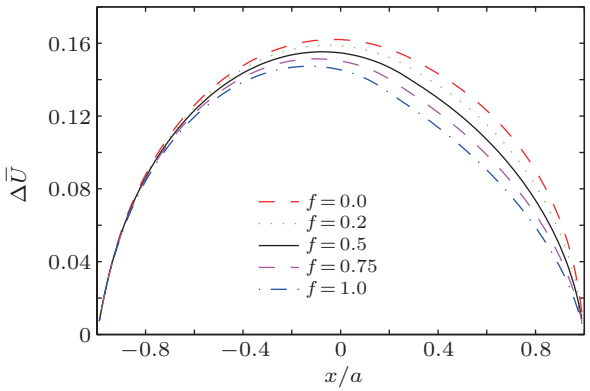


Fig. 14. (color online) Tangential shifts for $\alpha = 1$ and $\beta = 0.5$.

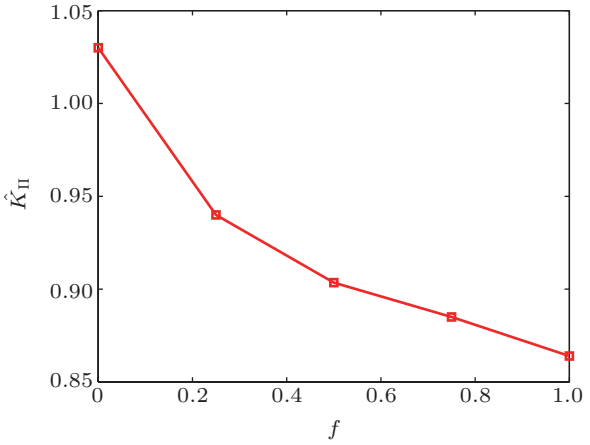


Fig. 15. (color online) Normalized stress intensity factor $\hat{K}_{\mathrm{II}}$ as a function of frictional coefficient f for $\alpha = 1$ and $\beta = 0.5$.

5. Conclusions

A node-pairs Lagrange multiplier method for modeling bimaterial interface crack face contact and friction was presented. The extent of the large-scale contact zones, displacements, and values for the mode II stress intensity factors were found to be in agreement with the previous analytical results. The effects of tension/shear ratios and Dundurs parameter β on contact zone sizes and the mode II stress intensity factors were found. Compared with the case where we ignore contact, the normalized mixed-mode stress-intensity factor at the right crack tip for considering contact is less than that of an embedded interface crack, which demonstrates that an error arises. When considering frictional contact, the normalized normal gap and the tangential shift decrease as the frictional coefficients increase. For $f = 1.0$, the mode II stress intensity factors decrease by 16% with respect to $f = 0$, and hence may be overestimated when neglecting frictional contact. The node-pairs Lagrange multiplier method can give accurate calculation result not only for the interface crack but also for the crack of homogeneous material. A center crack face on the cracked Brazilian disk specimens subjected to shear-compressive loading may be analyzed by this method.

References

[1] Clarkea D R, Oechsnera M and Padture N P 2012 *Mas. Bull.* **37** 891
[2] Wang G H and Zhang Y 2010 *Chin. Phys. B* **19** 127803
[3] Zhang Y K, Kong D J, Feng A X, Lu J Z, Zhang L H and Ge T 2006 *Acta Phys. Sin.* **55** 2897 (in Chinese)
[4] Padture N P, Gell M and Jordan E H 2002 *Science* **296** 280
[5] Evans A G, Mumm D R, Hutchinson J W, Meier G H and Pettit F S 2001 *Prog. Mater. Sci.* **46** 505
[6] Du G, Liu X Y, Xia Z L, Yang J F and Han R Q 2010 *Chin. Phys. B* **19** 057304
[7] He M Y, Hutchinson J W and Evans A G 2011 *J. Appl. Mech.* **78** 041008
[8] Pan H and Yang W T 2003 *Chin. Phys. Lett.* **20** 120
[9] Lotfy K H 2012 *Chin. Phys. B* **21** 014209
[10] Liu Z L, Hu H Y, Fan T Y and Xing X S 2010 *Chin. Phys. Lett.* **27** 106202
[11] Fan T Y and Li X F 2002 *Chin. Phys.* **11** 266
[12] Williams M L and Seismol B 1959 *J. Opt. Soc. Am.* **49** 199
[13] Erdogan F 1965 *J. Appl. Mech.* **32** 403
[14] England A H 1965 *J. Appl. Mech.* **32** 400
[15] Shih C and Asaro R 1989 *Mater. Sci. Eng. A* **107** 145
[16] Comninou M and Schmueser D 1979 *J. Appl. Mech.* **46** 345
[17] Gautesen A K 1993 *Int. J. Fract.* **60** 349
[18] Gautesen A K 1988 *J. Appl. Mech.* **55** 580
[19] van der Zande H D and Grootenboer H J 1986 *J. Appl. Mech.* **53** 573
[20] Lee J and Gao H 1995 *Int. J. Numer. Meth. Eng.* **38** 2465
[21] Giner E, Tur M and Tarancn J E 2010 *Int. J. Numer. Meth. Eng.* **82** 1424
[22] Elguedj T, Gravouil A and Combescure A 2007 *Int. J. Numer. Meth. Eng.* **71** 1569
[23] Zhu B, Wang C G, Cai H S and Cai X 2003 *Acta Phys. Sin.* **52** 1960 (in Chinese)
[24] Dorogoy A and Banks-Sills L 2004 *Int. J. Numer. Meth. Eng.* **59** 1749
[25] Wang C H 1997 *Eng. Fract. Mech.* **65** 77
[26] Laursen T A 2002 *Computational Contact and Impact Mechanics* (Berlin/Heidelberg: Springer-Verlag) p. 356
[27] Kim J O and Kwak B M 1996 *Int. J. Solids Struct.* **33** 4605
[28] Simo J C and Laursen T A 1992 *Comput. Struct.* **42** 97
[29] Kalarbring A and Bjorkirnan G 1988 *Comput. Struct.* **30** 1185
[30] Nicholas J C, Robert L T and Michael G K 1991 *Int. J. Numer. Meth.* **32** 103
[31] Wang X C 2003 *Finite Element Method* (Beijing: Tsinghua University Press) pp. 55–65 (in Chinese)
[32] Zienkiewicz O C, Taylor R L and Zhu J Z 2005 *The Finite Element Method: Its Basis and Fundamentals*, 2nd edn. (New York: Elsevier/Butterworth-Heinemann) pp. 201–220
[33] Chen W H and Tsai P 1986 *Comput. Struct.* **22** 925
[34] Giner E, Sabsabi M and Fuenmayor F J 2011 *Eng. Fract. Mech.* **78** 428
[35] Sun C T and Qian W 1988 *Int. J. Fract.* **94** 371